Unconventional Superconductivity in YPtBi and Related Topological Semimetals

Markus Meinert*
Center for Spinelectronic Materials and Devices, Bielefeld University, D-33501 Bielefeld, Germany
(Received 23 October 2015; revised manuscript received 28 January 2016; published 1 April 2016)

YPtBi, a topological semimetal with a very low carrier density, was recently found to be superconducting below $T_c = 0.77$ K. In conventional theory, the nearly vanishing density of states around the Fermi level would imply a vanishing electron-phonon coupling and would, therefore, not allow for superconductivity. Based on relativistic density-functional theory calculations of the electron-phonon coupling in YPtBi, it is found that carrier concentrations of more than 10^{21} cm^{-3} are required to explain the observed critical temperature with the conventional pairing mechanism, which is several orders of magnitude larger than experimentally observed. It is very likely that an unconventional pairing mechanism is responsible for the superconductivity in YPtBi and related topological semimetals with half-Heusler structure.

DOI: 10.1103/PhysRevLett.116.137001

A series of half-Heusler compounds with heavy elements were predicted to have a topologically nontrivial band order [1–3]. These compounds have a high cubic symmetry; however, they are without inversion symmetry. The normal band order—with the s-like, twofold-degenerate Γ_6 state sitting above the p-like, fourfold-degenerate Γ_8 state—is inverted in some of these compounds due to spin-orbit coupling. In their natural state, the cubic symmetry leads to a band degeneracy at Γ around the Fermi level, rendering them semimetals with a topologically nontrivial band order (topological semimetals) and very low density of states (DOS) at the Fermi level $D(E_F)$. By breaking the cubic symmetry with some amount of uniaxial strain, the compounds can be made insulating, and thus could become 3D topological insulators [4]. They would exhibit metallic surface states with Dirac-like dispersion; i.e., the electrons would behave as massless particles with ultrahigh mobility, while at the same time they would be insulating in the bulk. These surface states are topologically protected as long as time-reversal symmetry is preserved; i.e., they are protected against scattering from nonmagnetic impurities. Indeed, for some of these materials there is experimental evidence for topologically nontrivial band structures and the presence of Dirac surface states [5–7], although none were found to be insulating in the bulk. Some compounds from this class were found to be superconductors with critical temperatures up to 1.8 K, e.g., LaPtBi, LuPtBi, LuPdBi, YPtBi, and YPdBi [8–12]. Compounds of the type RPdBi (R is a lanthanide with an open $4f$ shell) that show coexisting local-moment antiferromagnetism as well as superconductivity have also been found; these point to the presence of spin-triplet Cooper pairs [12], which is allowed due to the missing structural inversion symmetry [13]. Because of the topologically nontrivial band structure, novel collective excitations are possible, including in particular surface Majorana fermions [14]. These could provide the basis for low-decoherence quantum processing [15].

Superconducting semiconductors such as GeTe and SnTe have long been known [16,17]; their superconductivity can be explained [17] with the Eliashberg theory of electron-phonon mediated superconductivity. $SrTiO_{3-x}$, the most dilute semiconductor known to date, has $T_c \lesssim 0.5$ K, and its superconductivity cannot be explained by simple electron-phonon coupling [18,19]. Instead, a plasmon-assisted mechanism was proposed to explain the unusual dependence of T_c on the carrier density [20]. The well-known expression for the superconducting transition temperature $k_B T_c = 1.13\hbar\omega_c \exp\left[-1/D(E_F)V\right]$ is obtained from the Bardeen-Cooper-Schrieffer theory, where ω_c is a cutoff frequency often identified with the Debye frequency and V is the effective interaction potential. Thus, the critical temperature is expected to increase with increasing $D(E_F)$. This expectation was confirmed for GeTe and SnTe, but in these materials T_c is limited to a few hundred mK [17]. More recently, superconductivity just below $T_c \approx 4$ K was discovered in highly B-doped diamond [21] and in $Cu_xBi_2Se_3$ [22], a prototype topological insulator for $x = 0$. For the latter case, it was shown by first-principles calculations of the electron-phonon coupling that the conventional pairing mechanism is most likely not strong enough to give rise to the rather high observed critical temperature [23]. Furthermore, the possibility of superconductivity in the surface states of topological insulators was recently explored [24,25], and it was shown that surface electron-phonon interaction can be strong.

Naturally the question arises whether the superconductivity in the topological half-Heusler compounds is of the conventional, phonon-mediated type. To shed some light on this question, first-principles calculations of the electron-phonon coupling for a topological semimetal from the half-Heusler class are presented in this Letter. The compound YPtBi, a bulk superconductor with a critical temperature of $T_c = 0.77$ K, was chosen as a representative member of this class [9,26–28].

The calculations were carried out with the Quantum Espresso distribution [29] within the framework of density-functional theory (DFT). Relativistic projector augmented-wave (PAW) potentials [30] (including spin-orbit coupling (SOC)] from PSlibrary [31] were employed, with kinetic energy cutoffs of 40 Ry for the wave functions and 400 Ry for the charge density. The results were checked against all-electron calculations, including SOC, with the full-potential linearized augmented plane-wave (FLAPW) method using the ELK code [32] and were found to agree very well. The Perdew-Burke-Ernzerhof (PBE) generalized gradient approximation was used for the exchange-correlation energy and potential. Since YPtBi is a semimetal, the use of a semilocal potential to describe the band structure is justified. The dynamical matrices and electron-phonon matrix elements $g^{\mathbf{q}\nu,mn}_{\mathbf{k}+\mathbf{q},\mathbf{k}}$ with phonon mode index ν and band indices m, n were obtained with density-functional perturbation theory on a $5\times5\times5$ $\mathbf{q}$-point mesh and $10\times10\times10$ $\mathbf{k}$-point mesh. Electron-phonon coupling was calculated by applying an interpolation scheme as described in Ref. [33]. The Eliashberg spectral function

$$\alpha^2F(\omega)=\frac{1}{D(E_F)}\sum_{mn}\sum_{\mathbf{q}\nu}\sum_{\mathbf{k}}\delta(\omega-\omega_{\mathbf{q}\nu})|g^{\mathbf{q}\nu,mn}_{\mathbf{k}+\mathbf{q},\mathbf{k}}|^2\times\delta(E_{\mathbf{k}+\mathbf{q},m}-E_F)\delta(E_{\mathbf{k},n}-E_F) \quad (1)$$

was evaluated on 40^3 $\mathbf{k}$-point and 20^3 $\mathbf{q}$-point meshes. The spectral function was obtained for several widths of a Gaussian approximation for the δ function between 0.004 and 0.02 Ry. The resulting density of states $D(E_F)$ and electron-phonon coupling constant λ, where

$$\lambda=2\int\frac{\alpha^2F(\omega)}{\omega}d\omega, \quad (2)$$

were extrapolated with a linear fit to the $\delta\to0$ limit. Convergence tests suggest that the accuracy for λ is of the order ±0.02. The superconducting gap Δ was calculated by solving the isotropic Eliashberg equations self-consistently as a function of temperature with a routine implemented in the ELK code [32], which is based on a similar algorithm described in Ref. [34]. The critical temperature T_c was obtained by interpolating $\Delta(T)$ with cubic splines and finding the inflection point. Additionally, the McMillan-Allen-Dynes formula

$$T_c=\frac{\omega_{\log}}{1.2}\exp\left[-\frac{1.04(1+\lambda)}{\lambda-\mu^*(1+0.62\lambda)}\right], \quad (3)$$

with the logarithmic average phonon frequency $\omega_{\log}$ and the screened Coulomb pseudopotential μ^*, was evaluated for comparison [35]. The Coulomb pseudopotential is usually taken as a parameter of the order $\mu^*=0.1,\ldots,0.2$, which we set to zero for the evaluation of the Eliashberg equations and the McMillan-Allen-Dynes equation; i.e., Coulomb repulsion is completely neglected. Thus, the critical temperatures obtained here are upper bounds for the electron-phonon-induced superconductivity. Doping was treated in a rigid-band approximation by adding or subtracting electrons from the band structure and compensating for this by adding a homogeneous background charge. The experimental lattice constant of 6.65 Å was used in all calculations. In systems with very low Fermi energy ($E_F\lesssim\omega_{\log}$), vertex corrections should in principle be included; this was shown to increase T_c to some extent [36]. However, for all carrier densities considered here we have $E_F\gg\omega_{\log}$; thus, the Eliashberg equations are expected to properly describe the electron-phonon interaction in YPtBi.

For an accurate description of the electron-phonon coupling, we need to make sure that the calculated band structure close to E_F is in agreement with the observed one. In the following, the computed electronic properties will be compared to experimental data to assess the validity of the band structure calculations. In Fig. 1 we plot the DOS, atom-projected DOS, band structure along high-symmetry lines, and the Fermi surface. The relativistic PAW and FLAPW calculations are in excellent agreement, establishing that the PAW method with the potentials from PSlibrary gives reliable results for YPtBi. The band structure plot clarifies that YPtBi has weakly overlapping bands close to the Brillouin zone center, making it a semimetal. The Fermi surface consists of two hole pockets and two sets of electron pockets, which belong to the fourfold-degenerate Γ_8 representation [3]. As shown in Ref. [3], the Γ_6 states lie below Γ_8, so that the band order is topologically nontrivial. The hole pockets are of approximately cubic

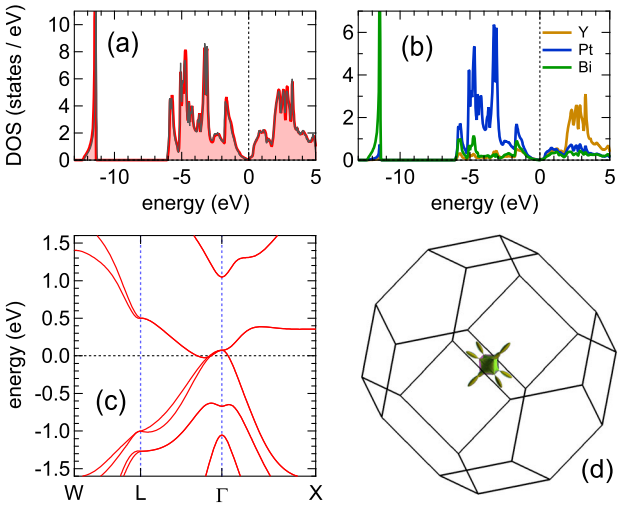

FIG. 1. (a) Density of states, (b) atom-projected density of states, (c) band structure, and (d) Fermi surface of YPtBi obtained from FLAPW calculations. DOS plots obtained from the relativistic PAW (thin gray) and FLAPW (thick red) calculations are compared in (a) to show the equivalence of the two methods.

shape centered around the zone center with corners along the Λ path. The inner hole pocket has a complex concave-convex shape and touches the outer hole pocket on the Λ and Δ paths. The electron pockets form a set of cigar-shaped ellipsoids with eightfold symmetry along the Λ paths. The small Fermi surface is in agreement with the small density of states at the Fermi energy of $D(E_F) = 0.038$ states/eV. The calculated $D(E_F)$ agrees very well with the value obtained from a heat capacity measurement, $D(E_F) \lesssim 0.042$ states/eV [37].

The Fermi surface obtained for YPtBi is remarkably similar to the Fermi surface of LaPtBi [38]. The Fermi vector in the [001] direction is $k_F^{[001]} \approx 0.033 a_0^{-1}$, and the volume enclosed by the two hole pockets is approximately $V_F^h \approx 0.000575 a_0^{-3}$. The corresponding carrier density is $n_e = n_h = 3 \times 10^{19}$ cm^{-3}. Recently, Shubnikov–de Haas (SdH) oscillations in YPtBi single crystals with the magnetic field along the [001] direction were observed with a frequency of $\Delta B^{-1} = 0.022$ T^{-1} [26], indicating that the true Fermi surface cross section is actually three times smaller than the calculated one. For the latter, a frequency of SdH oscillations with a periodicity of $\Delta B^{-1}_{[001]} \approx 0.0061$ T^{-1} is expected. Thus, the dip of the conduction band minimum below the valence band maximum on the Λ path is in fact not as deep as calculated. A beating node in the measurement indicates that there are two similar-sized Fermi surfaces contributing to the SdH oscillations, in perfect agreement with the band structure calculation. Simultaneous Hall effect measurements were analyzed with a one-band model, giving $n_h = 2 \times 10^{18}$ cm^{-3}. Based on the observed cross section of the Fermi surface and assuming a cubic shape, one obtains an enclosed charge density of $n_h \approx 4 \times 10^{18}$ cm^{-3}, which agrees nicely with the Hall effect measurement; however, it neglects multiband effects, different mobilities, and carrier compensation. This result supports the possibility that the true Fermi surface is much smaller than the calculated one. The surface-averaged effective masses on the calculated Fermi surface are $m_h^* = 0.2 m_e$ and $m_e^* = 0.41 m_e$ for the hole and electron pockets, respectively, where m_e is the free-electron mass. The hole effective mass is roughly in agreement with the value extracted from SdH oscillation, $m_h^* = 0.15 m_e$ [26]. Indeed, the DFT electronic structure calculation with the PBE functional reproduces the experimental observations very well up to a small error in the overlap between conduction and valence bands. Thus, the calculated electronic structure provides a solid foundation for the evaluation of the electron-phonon coupling discussed below.

The phonon density of states and the heat capacity of YPtBi are shown in Fig. 2. A clear separation of acoustic and optical modes is visible. From the low-temperature part of the heat capacity, a Debye temperature of $\Theta_D = 208$ K is obtained, in good agreement with the experimental value of 195(5) K [37]. Because of the small Fermi surface, only

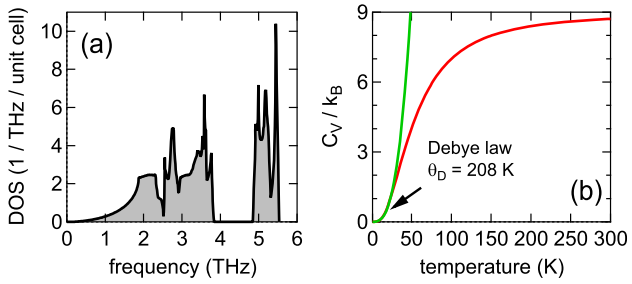

FIG. 2. Phonon density of states (a) and derived heat capacity (b) of pristine YPtBi.

very short $\mathbf{q}$-vectors with $q \leq 2k_F$ can connect different parts of the surface, which gives rise to the scattering of an electron state into another. Thus, the electron-phonon coupling is limited to a small region close to the zone center. From the extrapolation scheme for the Brillouin zone integration $\lambda = 0.02 \pm 0.02$ is obtained, which is obviously at the limit of the numerical accuracy of the Brillouin zone sampling. Certainly λ is small, but a more accurate λ will require an unfeasibly dense $\mathbf{q}$-point mesh. With $\mu^* = 0$, the solution of the Eliashberg equations shows that $T_c < 0.001$ K, which is much smaller than the observed critical temperature of $T_c = 0.77$ K.

To investigate the effect of doping, electron-phonon coupling was evaluated for doping levels of $\Delta n_e = \pm 1.0$ electrons per primitive cell. The dynamical matrices were recomputed for each doping level, so that phonons were treated at full self-consistency with respect to doping. The corresponding densities of states and Fermi energy shifts are given in Figs. 3(a) and 3(b). Because of the low DOS close to E_F in the undoped YPtBi, even small doping levels give rise to large Fermi energy shifts. As seen in Fig. 3(e), T_c is increased with an increase in both electron- and hole-type doping; however, electron doping ($\Delta n_e > 0$) is clearly more effective. The coupling leads to a renormalization of the phonon frequencies, which is indicated by the reduction of the Debye temperature, Fig. 3(d). This also indicates that YPtBi could be dynamically unstable at strong doping.

The observed critical temperature of $T_c = 0.77$ K is obtained at $\Delta n_e \approx +0.2 = 2.8 \times 10^{21}$ cm^{-3} or $\Delta n_e \approx -0.5 = 7 \times 10^{21}$ cm^{-3} with $\mu^* = 0$, see Fig. 3(e). These concentrations are lower bounds, because T_c decreases with $\mu^* > 0$. As seen in Fig. 3(e), the McMillan-Allen-Dynes formula closely resembles the full numerical solution of the Eliashberg equations, and it remains valid down to $T_c \approx 0.02$ K. In all cases, the Bardeen-Cooper-Schrieffer expression for the superconducting gap, $2\Delta(0) = 3.528 k_B T_c$, is approximately fulfilled by the numerical solutions. In addition, the usual relation of λ with the renormalization function $Z(\omega = 0) = 1 + \lambda$ was found to be fulfilled in all cases, which demonstrates the consistency of the Eliashberg calculations.

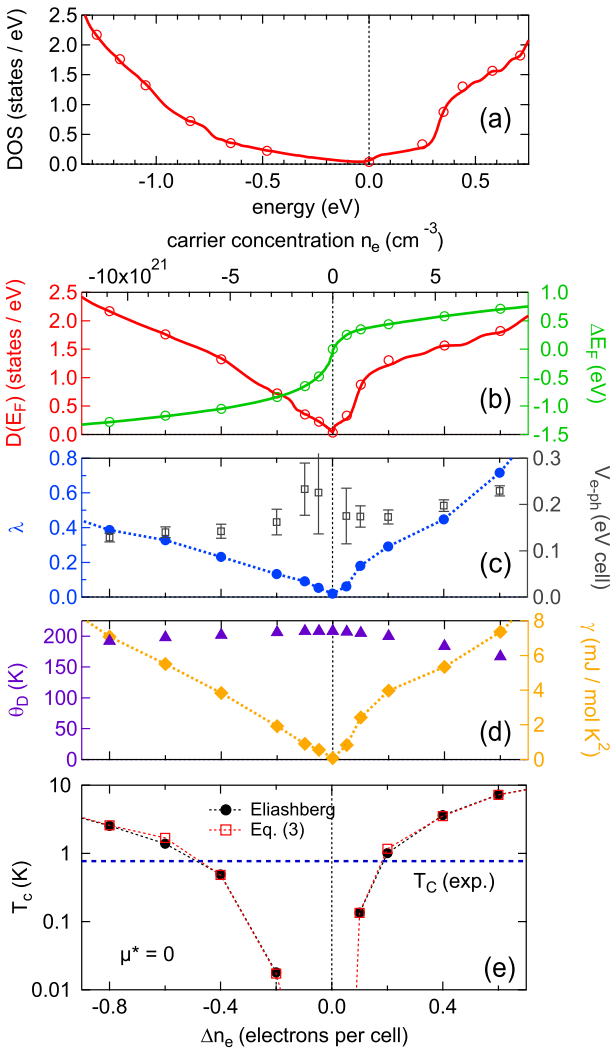

FIG. 3. (a) Density of states as a function of the energy. Open circles mark the values for which electron-phonon calculations were done. (b) Density of states and Fermi energy shift as a function of additional electrons per primitive cell Δn_e. (c) and (d) Electron-phonon coupling constant λ, interaction potential $V_{e\text{-ph}} = \lambda/(1+\lambda)D(E_F)^{-1}$, Debye temperature Θ_D, and Sommerfeld coefficient γ as functions of Δn_e. (e) Calculated critical temperatures from the numerical solution of the Eliashberg equations and from the McMillan-Allen-Dynes formula.

To study the influence of $D(E_F)$, the electron-phonon interaction potential $V_{e\text{-ph}} = \lambda/(1+\lambda)D(E_F)^{-1}$ is given in Fig. 3(c). Over the full range of doping concentrations, the interaction potential is $V_{e\text{-ph}} \approx 0.2$ eV cell, so the low value of λ for weakly and undoped YPtBi comes mainly from the low $D(E_F)$, or, equivalently, from the small Fermi surface area. These doping levels could be realized through off-stoichiometry (YPtBi crystals are mostly grown out of Bi flux, so additional Bi could easily be incorporated), or locally due to a site swap between neighboring cells. In addition, grain boundaries and other inhomogeneities with different stoichiometry could serve as sources of intrinsic doping. However, the carrier concentrations required for the electron-phonon coupling to be strong enough to explain the observed critical temperature are at least one order of magnitude larger than the typically observed carrier concentrations in YPtBi, and are three orders of magnitude larger than the samples with lowest observed carrier concentration (2×10^{18} cm^{-3}, Ref. [26]). Because of the increase in $D(E_F)$ the Sommerfeld coefficient of the heat capacity, $\gamma = \pi^2 D(E_F)(1+\lambda)k_B^2/3$, would increase to values around $\gamma \approx 4$ mJ/mol K^2 [see Fig. 3(d)], much larger than the measured value of $\gamma \lesssim 0.1$ mJ/mol K^2 [37]. Experiments with high-quality samples indicate that the normal-state electronic properties of YPtBi are perfectly in agreement with the calculation for the ideal, undoped case [26,27]. A diamagnetic screening fraction of around 70% was observed in the superconducting state, underlining that a large part of the material is in the superconducting state; this thereby rules out the possibility of grain-boundary superconductivity [28] or surface superconductivity [24]. The calculated critical temperature in the experimentally observed carrier concentration range of 2×10^{18} cm^{-3} to 4.2×10^{20} cm^{-3} [9,26–28] is $T_c \ll 0.1$ K. However, an even more remarkable observation is that the experimental critical temperature of YPtBi varies little across different samples, despite the carrier concentrations varying over two orders of magnitude. From Fig. 3(e), one would expect to have a variation of T_c over several orders of magnitude in that range.

The lack of a clear correlation between normal-state electronic properties, sample quality, and critical temperature indicates that the electron-phonon interaction induced by doping is not an explanation for the superconductivity in YPtBi. The relation between critical field and temperature observed in Ref. [27] deviates from conventional s-wave behavior and suggests that the material could be a p-wave superconductor, very similar to $Cu_xBi_2Se_3$. On the other hand, Cooper pair wave functions with angular orbital momentum $l > 0$ are not protected by the Anderson theorem; thus, random scattering from defects and impurities should reduce T_c if the elastic mean free path ℓ is smaller than the superconducting coherence length ξ [39]. Values of $\xi = 15$ and 17 nm and $\ell = 105$ and 130 nm were observed for YPtBi [26,27], but superconductivity was also reported in a case where the mean free path based on free-electron theory, i.e., $\ell = \hbar k_F/\rho_0 n e^2$ where $k_F = (3\pi^2 n)^{1/3}$ is smaller than the lattice constant [9]. This indicates that YPtBi is superconducting even in the dirty limit, which apparently contradicts the hypothesis of p-wave superconductivity. A remarkable side note is that many half-Heusler compounds are known to be semiconductors that show large thermoelectric power at appropriate doping. Even though the carrier concentrations are often high, superconductivity has never been reported for any of these compounds [40].

Based on the analysis of the electron-phonon coupling and the comparison with experimental data on the normal-state properties, it is safe to conclude that an unconventional mechanism is responsible for the superconductivity in YPtBi. Related compounds from the class of topological half-Heusler semimetals, *R*PtBi and *R*PdBi (with a rare-earth element *R*), have very similar normal-state properties as YPtBi and also show superconductivity with critical temperatures up to 1.8 K. It is most likely that an unconventional pairing mechanism is at work in all of these compounds. More experimental work, in particular careful studies on the interplay between structural order, normal-state electronic properties, and superconductivity are necessary to obtain more systematic knowledge about the pairing mechanism and the parity of the Cooper pairs. From the theoretical point of view, it is particularly challenging to identify pairing mechanisms that allow for sufficiently strong coupling despite the low Fermi density of states, one example of which is an electron-electron coupling assisted by plasmons [20].

Calculations leading to the results presented in this Letter were performed in part with resources provided by the Paderborn Center for Parallel Computing. The author thanks Thomas Dahm for fruitful discussions.

*meinert@physik.uni-bielefeld.de

[1] H. Lin, L. A. Wray, Y. Xia, S. Xu, S. Jia, R. J. Cava, A. Bansil, and M. Z. Hasan, Nat. Mater. **9**, 546 (2010).
[2] W. Al-Sawai, H. Lin, R. S. Markiewicz, L. A. Wray, Y. Xia, S. Y. Xu, M. Z. Hasan, and A. Bansil, Phys. Rev. B **82**, 125208 (2010).
[3] W. Feng, D. Xiao, Y. Zhang, and Y. Yao, Phys. Rev. B **82**, 235121 (2010).
[4] X.-L. Qi and S.-C. Zhang, Rev. Mod. Phys. **83**, 1057 (2011).
[5] C. Liu, Y. Lee, T. Kondo, E. D. Mun, M. Caudle, B. N. Harmon, S. L. Budko, P. C. Canfield, and A. Kaminski, Phys. Rev. B **83**, 205133 (2011).
[6] C. Shekhar, S. Ouardi, A. K. Nayak, G. H. Fecher, W. Schnelle, and C. Felser, Phys. Rev. B **86**, 155314 (2012).
[7] B. Nowak, O. Pavlosiuk, and D. Kaczorowski, J. Phys. Chem. C **119**, 2770 (2015).
[8] G. Goll, M. Marz, A. Hamann, T. Tomanic, K. Grube, T. Yoshino, and T. Takabatake, Physica (Amsterdam) **403B**, 1065 (2008).
[9] C. Shekhar, M. Nicklas, A. K. Nayak, S. Ouardi, W. Schnelle, G. H. Fecher, C. Felser, and K. Kobayashi, J. Appl. Phys. **113**, 17E142 (2013).
[10] F. F. Tafti, T. Fujii, A. Juneau-Fecteau, S. Rene de Cotret, N. Doiron-Leyraud, A. Asamitsu, and L. Taillefer, Phys. Rev. B **87**, 184504 (2013).
[11] G. Xu, W. Wang, X. Zhang, Y. Du, E. Liu, S. Wang, G. Wu, Z. Liu, and X. X. Zhang, Sci. Rep. **4**, 5709 (2014).
[12] Y. Nakajima, R. Hu, K. Kirshenbaum, A. Hughes, P. Syers, X. Wang, K. Wang, R. Wang, S. R. Saha, D. Pratt, J. W. Lynn, and J. Paglione, Sci. Adv. **1**, e1500242 (2015).
[13] M. Sigrist, D. F. Agterberg, P. A. Frigeri, N. Hayashi, R. P. Kaur, A. Koga, I. Milat, K. Wakabayashi, and Y. Yanase, J. Magn. Magn. Mater. **310**, 536 (2007).
[14] M. Sato and S. Fujimoto, Phys. Rev. B **79**, 094504 (2009).
[15] M. Leijnse and K. Flensberg, Semicond. Sci. Technol. **27**, 124003 (2012).
[16] R. A. Hein, J. W. Gibson, R. Mazelsky, R. C. Miller, and J. K. Hulm, Phys. Rev. Lett. **12**, 320 (1964).
[17] P. B. Allen and M. L. Cohen, Phys. Rev. **177**, 704 (1969).
[18] J. F. Schooley, W. R. Hosler, E. Ambler, J. H. Becker, M. L. Cohen, and C. S. Koonce, Phys. Rev. Lett. **14**, 305 (1965).
[19] E. Bustarret, Physica (Amsterdam) **514C**, 36 (2015).
[20] Y. Takada, J. Phys. Soc. Jpn. **49**, 1267 (1980).
[21] E. A. Ekimov, V. A. Sidorov, E. D. Bauer, N. N. Mel'nik, N. J. Curro, J. D. Thompson, and S. M Stishov, Nature (London) **428**, 542 (2004).
[22] Y. S. Hor, A. J. Williams, J. G. Checkelsky, P. Roushan, J. Seo, Q. Xu, H. W. Zandbergen, A. Yazdani, N. P. Ong, and R. J. Cava, Phys. Rev. Lett. **104**, 057001 (2010).
[23] X.-L. Zhang and W.-M. Liu, Sci. Rep. **5**, 8964 (2015).
[24] S. Das Sarma and Q. Li, Phys. Rev. B **88**, 081404 (2013).
[25] D. Li, B. Rosenstein, B. Y. Shapiro, and I. Shapiro, Phys. Rev. B **90**, 054517 (2014).
[26] N. P. Butch, P. Syers, K. Kirshenbaum, A. P. Hope, and J. Paglione, Phys. Rev. B **84**, 220504 (2011).
[27] T. V. Bay, T. Naka, Y. K. Huang, and A. de Visser, Phys. Rev. B **86**, 064515 (2012).
[28] T. V. Bay, M. Jackson, C. Paulsen, C. Baines, A. Amato, T. Orvis, M. C. Aronson, Y. K. Huang, and A. de Visser, Solid State Commun. **183**, 13 (2014).
[29] P. Giannozzi *et al.*, J. Phys. Condens. Matter **21**, 395502 (2009).
[30] A. Dal Corso, Phys. Rev. B **82**, 075116 (2010).
[31] A. Dal Corso, Comput. Mater. Sci. **95**, 337 (2014).
[32] http://elk.sourceforge.net.
[33] M. Wierzbowska, S. de Gironcoli, and P. Giannozi, arXiv: cond-mat/0504077v2.
[34] E. R. Margine and F. Giustino, Phys. Rev. B **87**, 024505 (2013).
[35] P. B. Allen and R. C. Dynes, Phys. Rev. B **12**, 905 (1975).
[36] Y. Takada, J. Phys. Chem. Solids **54**, 1779 (1993).
[37] P. G. Pagliuso, C. Rettori, M. E. Torelli, G. B. Martins, Z. Fisk, J. L. Sarrao, M. F. Hundley, and S. B. Oseroff, Phys. Rev. B **60**, 4176 (1999).
[38] T. Oguchi, Phys. Rev. B **63**, 125115 (2001).
[39] A. P. Mackenzie and Y. Maeno, Rev. Mod. Phys. **75**, 657 (2003).
[40] T. Graf, C. Felser, and S. S. P. Parkin, Prog. Solid State Chem. **39**, 1 (2011).